# Performance Evaluation of a Flexible Rotor in Extreme Ground Effect

Mor Gilad*     Inderjit Chopra†     Omri Rand‡

Alfred Gessow Rotorcraft Center
Department of Aerospace Engineering
University of Maryland
College Park, MD 20742, USA

### Abstract

Ground effect on hovering rotor performance has been widely studied both experimentally and theoretically, yet most applications have focused on global thrust and power values. Motivated by the Sikorsky Human Powered Helicopter Challenge (HPH), an attempt to further study ground influence on a hovering rotor of highly elastic blades in extreme ground proximity has been carried out. The experimental portion of this study includes both a rigid blade sub-scale set-up and elastic blade full scale set-up. Experimental results are used to validate a new computational tool that couples rigid prescribed wake, blade element aerodynamics and finite-element structural modeling, tailored together for prediction of elastic blade behavior in ground effect. The current model accounts for local height off the ground at each blade element, and allows for more detailed insight regarding angle of attack, induced velocities and lift distributions along the blade in extreme ground effect conditions.

### Nomenclature

| | |
|---|---|
| $\tilde{(\;)}$ | Property non-dimensionalized by R |
| $\vec{(\;)}$ | Vector property |
| $(\;)_{NW}$ | Property referenced to near wake |
| $(\;)_{FW}$ | Property referenced to far wake |
| $(\;)_{OGE}$ | Property referenced out of ground effect |
| $(\;)_{IGE}$ | Property referenced in ground effect |
| $A$ | Rotor disk area, $\pi R^2$ |
| $c$ | Rotor blade chord |
| $C_d$ | Section drag coefficient, $D/(\frac{1}{2}\rho U^2 c)$ |
| $C_l$ | Section lift coefficient, $L/(\frac{1}{2}\rho U^2 c)$ |
| $C_m$ | Section pitching moment coefficient, $M/(\frac{1}{2}\rho U^2 c)$ |
| $C_P$ | Rotor power coefficient, $P/(\rho A \Omega^3 R^3)$ |
| $C_Q$ | Rotor torque coefficient, $Q/(\rho A \Omega^3 R^2)$ |
| $C_T$ | Rotor thrust coefficient, $T//(\rho A \Omega^2 R^2)$ |
| HPH | Human Powered Helicopter |
| $L$ | Lift of a blade element |
| $N_b$ | Number of blades |
| $N_e$ | Number of blade elements |
| $N_{rev}$ | Number of far wake rotor revolutions |
| $P$ | Dimensional power |
| $\tilde{r}$ | Dimensionless radial coordinate along blade, $r/R$ |
| $\tilde{r}_{tip}$ | Tip vortex non-dimensional radial coordinate, $r_{tip}/R$ |
| $R$ | Rotor radius |
| $T$ | Dimensional thrust |
| $Z$ | Height above ground |
| $Z/R$ | Non-dimensional height above ground |
| $\tilde{z}_{tip}$ | Tip vortex non-dimensional axial coordinate, $z_{tip}/R$ |

| | |
|---|---|
| $\alpha$ | Effective Angle of attack |
| $\phi$ | Induced Angle of attack |
| $\Gamma$ | 2D Circulation per unit length |
| $\Gamma_{tip}$ | Tip vortex strength (circulation) |
| $\lambda$ | Non-dimensional inflow velocity |
| $\psi$ | Blade azimuthal angle |
| $\psi_w$ | Wake age |
| $\rho$ | Flow density |
| $\sigma$ | Rotor solidity, $N_b c/(\pi R)$ |
| $\theta$ | Collective pitch angle |
| $\theta_{tw}$ | Linear blade twist |
| $\Omega$ | Rotor rotational speed |

### Introduction

Recently, the Alfred Gessow Rotorcraft Center has been vigorously pursuing the Sikorsky Human Power Helicopter challenge, and has developed a quad-rotor system for this task. Each rotor consists of two blades of 6.5 $m$ radius which are ultra-lightweight and as such substantially flexible. Designed under the strict constraints of limited available human power, these rotors are intended for operation as close to the ground as possible in attempt to maximize ground effect benefits.

Influences of ground proximity on helicopter performance have been extensively studied since the 1940's through experiments [5–12] suggesting reduction as high as $30\% - 60\%$ in total power requirements when hovering close to the ground (Figure 1). Theoretical research efforts included analytical models [13], empirical curves [4,14,15], numerical wake computations based on free-vortex theory coupled with mirror images [16,17], CFD work [18], and phenomena-based models [19].

The direct influence of ground vicinity results is a decrease in inflow. This typically reflects in experiments by reduction

---
* Graduate Research Assistant. email: **mgilad@umd.edu**
† Alfred Gessow Professor and Director, email:**chopra@umd.edu**
‡ Visiting Professor, email:**omri@aerodyne.technion.ac.il**

in power required in-ground-effect relative to power required out-of-ground-effect ($P_{IGE}/P_{OGE}$) for constant thrust or corresponding augmentation in thrust for given power, both driven by dimensionless height $Z/R$. Since helicopter rotors do not generally hover lower than approximately $Z/R = 0.5$ due to fuselage height [7], experimental data for the extreme ground effect regime of $0.05 < Z/R < 0.5$ are scarce, and thus, extracted ground effect models are of low fidelity in this regime.
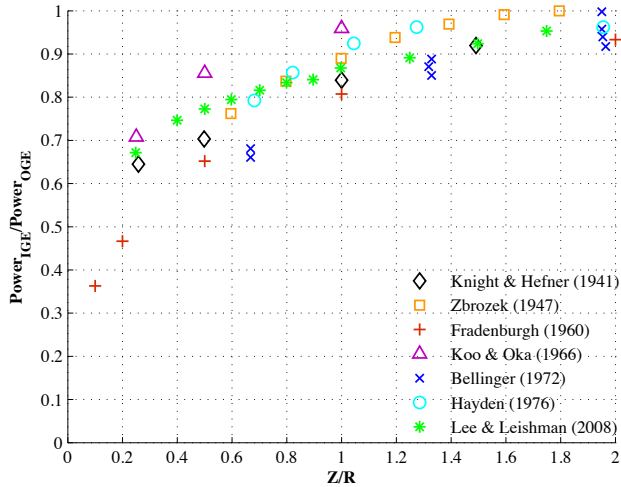


**Fig. 1: Ground effect influence on total power requirements for constant thrust, available results from literature**

Therefore, two new experiments dedicated to exploring this regime were designed and carried out in-house, providing a validation database for modeling rotor performance in extreme ground environment.

Previous works suggest utilizing existing trends mostly by multiplying global OGE predicted thrust or power values with some factor $f(Z/R)$ derived from experiments or models [2–4, 20] at a fixed $Z/R$ value, thus ignoring the influence of elasticity in ground effect. The goal of the present effort is to develop a predictive tool for performance evaluation of a highly elastic rotor in extreme ground effect, which captures the effect of variation in $Z(\tilde{r})/R$ along a substantially deflected blade. For this analysis, blade element theory is used in conjunction with a finite element model to account for blade bending and torsion, employing a newly configured prescribed IGE wake model.

## Ground Effect Experiments

The first experimental set-up presented in this study (shown in Figure 2) uses a sub-scale rotor consisting of two fairly rigid, untwisted, untapered, uniform NACA0012 blades, 1.37 $m$ in radius and 0.27 $m$ in chord. Blade pitch, RPM, and rotor height were varied, focusing on the extremely low $Z/R$ regime, while thrust and torque were measured using load and torque sensors respectively. For these settings, the rotor produces relatively low thrust values involving operational tip Reynolds number of 200,000. However, the drag coefficients at these Reynolds numbers are quite significant. For these reasons, it was important to verify the repeatability and accuracy of the experimental results, especially at the extremely low rotor heights.
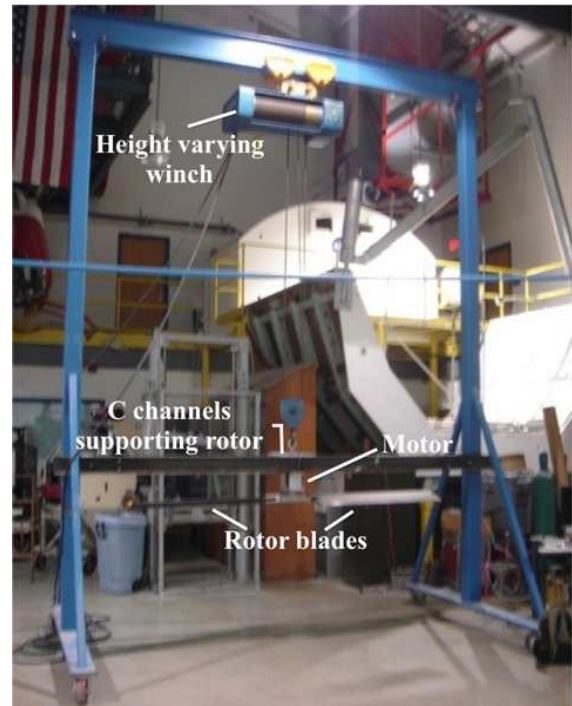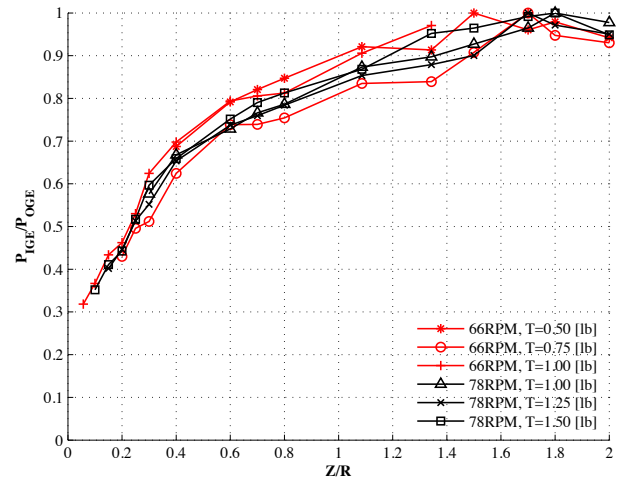


**Fig. 2: Sub scale ground effect test rig**



**Fig. 3: Sub scale test results showing total power ratio in ground effect for constant thrust**

Resulting $P_{IGE}/P_{OGE}$ ratios for constant thrust are shown in Figure 3 where significant power reductions, consistent with previous experiments (Figure 1), are evident at low heights ($Z/R < 0.4$). An averaged trend-line based on the newly generated test data from the rigid sub-scaled rotor was then compared to past results, all shown in Figure 4, and showed a very good overall agreement.

A second in-house experiment featured a large rotor designed towards a full-scale quad-rotor configuration. Each rotor consists of two ultra-lightweight, substantially flexible, untwisted, untapered blades, that measure 6.5 $m$ in radius and 1.0 $m$ in chord. This rotor is designed to operate in extremely low RPM ($10 \leq RPM \leq 20$) resulting in a tip Reynolds number range of $Re = 500,000 - 900,000$. The Eppler387 airfoil, designed for relatively low Reynolds number conditions [21], was
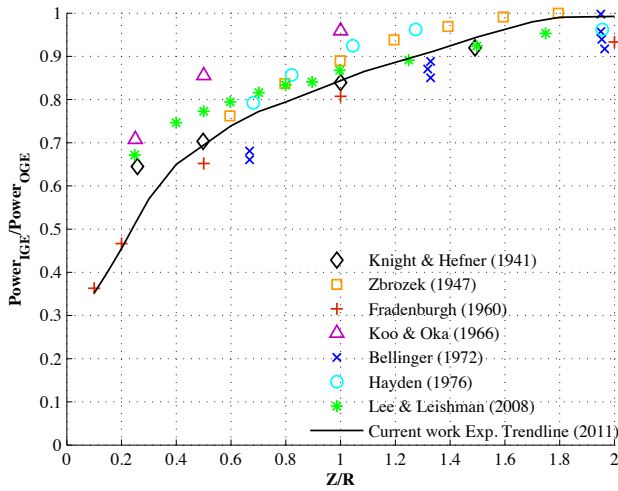
Fig. 4: Sub-scale test ground effect trend-line vs previous experimental results

selected for these blades. The test set-up was poised 0.6 $m$ off the ground (seen in Figure 5 ) as thrust and torque were measured for various settings of pitch and RPM. Tests were also carried out at 1.3 $m$ for a more comprehensive study of performance losses due to height off ground for flexible blades.



Fig. 5: Full scale ground effect test rotor

Representative results of data collected using this set-up at both heights are shown in Figure 6. Extremely high blade deflections were observed, approaching 1 $m$ at the tip for the maximum tested load. These deflections represent $(Z/R)_{tip} \approx 2.5(Z/R)_{hub}$ at the lower tested height setting of 0.6 $m$, while at the even lower HPH designed operational height of 0.3 $m$ these deflections translate to the significant difference of $(Z/R)_{tip} \approx 4(Z/R)_{hub}$. With careful modeling, consideration of these deflections might prove to be key in successful prediction of this rotor's performance.

## Prescribed Wake Formulation and Implementation in and out of Ground Effect

Due to the unusual characteristics of the HPH rotor operating environment (namely highly elastic blades, extremely low Z/R, and relatively low rotation speeds yielding relatively high $C_T$ values) a phenomenon-based method is proposed, where-in modeling wake behavior to calculate rotor performance in extreme ground effect. The proposed method is driven by a rigid prescribed wake analysis, tailored for these conditions, coupled with a mirror-image wake satisfying a no penetration condition at the ground (illustrated in Figure 7) and FEM analysis for blade bending and torsion accounting for blade deflections.
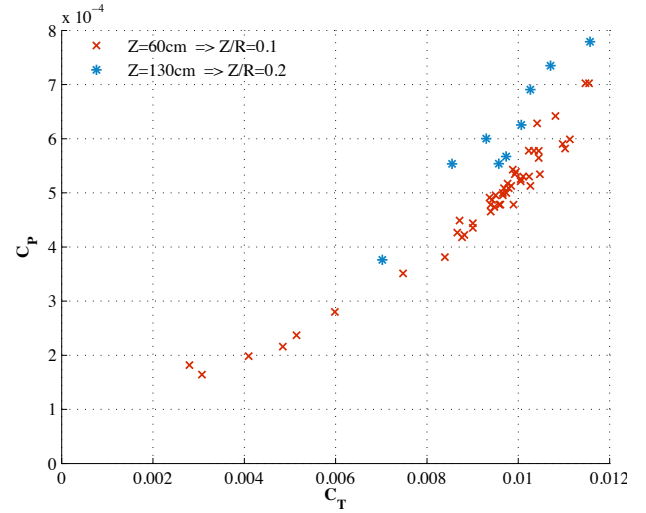


Fig. 6: Total power coefficient variation with thrust coefficient, for a highly elastic rotor in ground effect
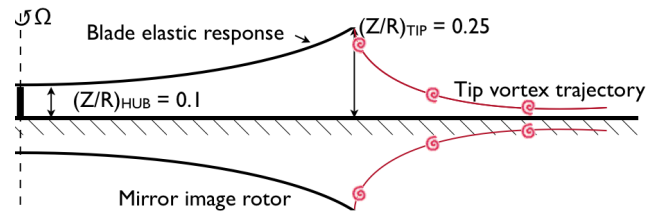


Fig. 7: Illustration of a highly elastic rotor blade in extreme ground effect with its mirror image

### General Prescribed Wake Formulation

As proposed by Landgrebe [22], each rotor blade is divided into a finite number of elements $N_e$, modeled by a single horseshoe vortix, following classical lifting line theory. Each horseshoe vortix is comprised of a bound segment at the quarter-chord and two trailing vortices located at the element boundaries comprising of the same circulation strength $\Gamma$. The rotor wake is then represented by two regions, near-wake and far-wake. The near wake, modeling the first 30° of the wake (following Johnson [15]), is comprised of the trailing vortices from each blade element, illustrated for representative 5 blade elements in Figure 8. Each trailing vortex is modeled by a finite number of straight vortex filaments of the same circulation strengths extending from the blade trailing edge and defined by wake azimuth intervals, $\Delta\psi$. The far wake is represented by a single tip vortex of constant circulation strength (one tip vortex for each blade), determined by the maximum circulation along the blade span [15]. Each tip vortex is considered for a finite number of $N_{rev}$ rotor revolutions (typically $N_{rev} = 10$ was found to be sufficient) and is divided into a finite number of straight vortex filaments.

The prescribed tip vortex trajectory, based on the work by Landgrebe [22, 23], later refined by Kocurek and Tangler [24], describes the locations of each rotor tip vortex in radial and axial coordinates as functions of wake age $\psi_w$ on the basis of multiple experimental observations.
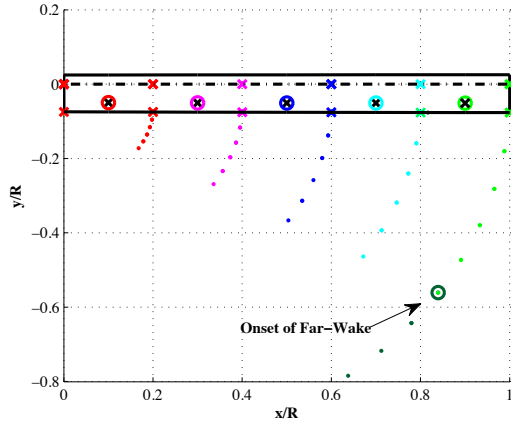
**Fig. 8: Illustration of Near-Wake modeling for 5 representative blade elements**

For a given wake trajectory, the circulation strength distribution $\overline{\Gamma}(\tilde{r})$ can be iteratively solved for, using an initial guess, via the following steps:

i. Defining tip vortex circulation strength $\Gamma_{tip} = max(\overline{\Gamma})$.

ii. Calculating far-wake induced velocities using Biot-Savart law and $\Gamma_{tip}$, so that for each blade element:

$$\bar{v}_{FW} = \begin{Bmatrix} v_x \\ v_y \\ v_z \end{Bmatrix}_{FW} \qquad (1)$$

iii. Obtaining expressions for near-wake induced velocities, in the form of coefficient matrices $[A_{NW}]$ calculated using Biot-Savart law and an unknown distribution $\overline{\Gamma}(\tilde{r})$, so that for each blade element :

$$\bar{v}_{NW} = \begin{Bmatrix} v_x \\ v_y \\ v_z \end{Bmatrix}_{NW} = \begin{Bmatrix} [A_{NW}]_x \\ [A_{NW}]_y \\ [A_{NW}]_z \end{Bmatrix} \cdot \overline{\Gamma} \qquad (2)$$

iv. Using both vectors of wake induced velocities and the local blade element velocity $\Omega\tilde{r}$, employ a no-penetration condition at the $3/4$ chord and mid span of each blade element, solving a system of $N_e$ equations for $\overline{\Gamma}(\tilde{r})$ - circulation strength distribution, so that in the direction normal to chord:

$$[A_{NW}(\tilde{r})] \cdot \overline{\Gamma}(\tilde{r}) + v_{FW}(\tilde{r}) - \Omega\tilde{r}\sin(\theta(\tilde{r})) = 0 \qquad (3)$$

The initial guess for $\Gamma_{tip}$ is based on the following approximation, assuming on a constant $\Gamma$ along the blade:

$$T = N_b \cdot \int_0^R \rho U \Gamma dr = N_b \cdot \int_0^R \rho \Omega r \Gamma dr = \frac{N_b}{2}\rho\Omega R^2 \Gamma \qquad (4)$$

Once the strengths of the wake vorticity have converged (defined when the maximum change in $\overline{\Gamma}(\tilde{r})$ does not exceed 0.01%), this distribution is used to calculate the corresponding aerodynamic lift coefficient using:

$$L(\tilde{r}) = \rho U \overline{\Gamma}(\tilde{r}) = \frac{1}{2}\rho U^2 c \cdot C_l(\tilde{r}) \qquad (5)$$

The angle of attack distribution can then be extracted via 2D aerodynamic tables using the $C_l$ distribution, subsequently providing $C_d$ and $C_m$ distributions. Forces and moments are integrated along the blade yielding thrust, torque, and power values. Finite element analysis is then carried out using the distributed loads to obtain blade deflections, defining the height and pitch of each blade element creating the $Z(\tilde{r})/R$ distribution along the blade, and updating the geometry and control points of the modeled shed vortices.

To ensure sufficient convergence, sensitivity studies were carried out with respect to number of blade elements ($N_e$), azimuthal step ($\Delta\psi$), number of modeled tip vortex revolutions ($N_{rev}$) and the length of the near-wake modeled portion. It was found that for any combination of $N_e \geq 40$, $\Delta\psi \leq 5°$, $N_{rev} \geq 8$ and a near-wake length of $15° - 45°$ results for trim collective, power, and angle of attack, vary by less than 2%. All results in the current work make use of $N_e = 50$, $\Delta\psi = 5°$, $N_{rev} = 10$ and a near-wake trailing $30°$ behind the blade.

For OGE calculations, a prescribed wake model given in Kocurek and Tangler [24] was used, describing the tip vortex geometry using the equations:

$$\tilde{r}_{tip} = \frac{r_{tip}}{R} = 0.78 + (1 - 0.78)\exp(-4\sqrt{C_T}\psi) \qquad (6)$$

and -

$$\tilde{z}_{tip} = \frac{z_{tip}}{R} = \begin{cases} k_1\psi & \text{for } 0 \leq \psi \leq \frac{2\pi}{N_b} \\ k_1\frac{2\pi}{N_b} + k_2(\psi - \frac{2\pi}{N_b}) & \text{for } \frac{2\pi}{N_b} \leq \psi \end{cases} \qquad (7)$$

where:

$$k_1 = -0.000729\theta_{tw} + (-2.3 + 0.206\theta_{tw})\frac{(C_T)^m}{(N_b)^n} \qquad (8)$$

$$k_2 = -\sqrt{C_T - (N_b)^n \left( \frac{0.000729\theta_{tw}}{-2.3 + 0.206\theta_{tw}} \right)^{1/m}} \qquad (9)$$

and

$$m = 1 - 0.25\exp(0.04\theta_{tw}); \qquad n = 0.5 - 0.0172\theta_{tw} \qquad (10)$$

**Prescribed Wake Formulation in Ground Effect**
An implementation of the above formulation in ground effect required a new prescribed trajectory representing the wake behavior in this environment. Griffiths and Leishman [16] presented axial and radial displacements of the wake of a rotor at $Z/R = 0.62$ for 12 rotor revolutions. (Experimental results by Light [25] were also considered for this task, however results were shown only for the limited wake age of $250° - 450°$ while the current method required data for at least 8 revolutions.) The results of [16] were tailored with a curve-fit to provide analytical functions for $\tilde{z}(\psi)$ and $\tilde{r}(\psi)$, used as the baseline trajectory, and are shown (solid line) in Figure 9 and Figure 10.

Generalization of this trajectory was carried out employing the reference case where $C_T = 0.008$, $Z/R = 0.62$ as a baseline, focusing on the range of interest $Z/R \leq 0.6$ and under two main assumptions for this regime:

i. The wake trajectory shape depends on variation in $Z/R$ alone.

ii. The advancement rate along said trajectory (the tangential velocity) depends on $C_T$ alone.

Implementation of varying rotor height above ground was carried out assuming similarities in trajectory shapes. This assumption presumably breaks down at higher $Z/R$ values, where the radial coordinates are observed to contract more substantially before the ground induced wake expansion initiates [12]. A simple normalization of the reference case $\tilde{z}_{tip}(\psi)$ by its rotor hub height off ground allowed scaling the axial coordinates per $Z/R$ case, while maintaining the same radial coordinates. An example for $Z/R = 0.3$ is compared to the reference case of $Z/R = 0.62$ in Figure 9.
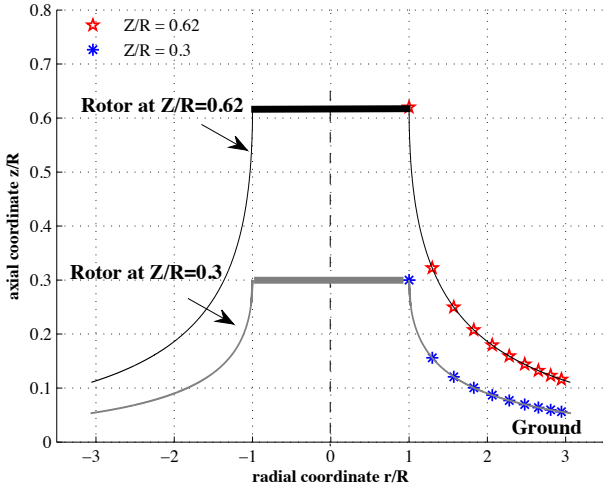


**Fig. 9: Effect of $Z/R$ on prescribed trajectory at $C_{T_{ref}} = 0.008$**

To include the effect of $C_T$ in the proposed wake model, experimental results for rotor wakes IGE from the works of Light [25] and Lee and Leishman [12] were carefully examined, showing that the velocity at the rotor plane, scales with $\sqrt{C_T}$, a result which is consistent with classical momentum theory [2, 15]. This was done by comparing non-dimensional distances (normalized by $R$) between the first and second tip vortices, varying from each other by $\psi = \pi$, yielding velocities. These comparisons are shown in Table 1. Using this result in conjunction with the fact that close to the rotor plane, the tangential velocity is dominated by axial (vertical) velocity, and the fact that vortex elements at the early wake ages also have the largest effect on performance calculations, the tangential velocities of the vortices along the prescribed trajectory are scaled with $\sqrt{C_T}$. This is carried out by using the reference case shape functions $\tilde{z}_{ref}(\psi)$, $\tilde{r}_{ref}(\psi)$, and scaling the 'time' coordinate $\psi$ to move 'faster' or 'slower' along the trajectory following the process described below:

i. For $C_{T_{req}} = C_{T_{ref}}$, for every azimuth in the reference case, $\psi_{ref}$, the tip vortex has traveled a certain distance. For relatively small wake ages, close to the rotor, this distance is traveled mainly in the axial direction, and is approximated as $\Delta \tilde{z}_{ref}$.

| $C_{T_{ref}} = 0.008$ | $C_{T_1} = 0.0154$ | $C_{T_2} = 0.0161$ | $C_{T_3} = 0.0196$ |
|---|---|---|---|
| $\sqrt{C_T/C_{T_{ref}}}$ | 1.39 | 1.42 | 1.56 |

| $(V/R)_{ref} = 0.055$ | $(V/R)_1 = 0.0772$ | $(V/R)_2 = 0.0779$ | $(V/R)_3 = 0.088$ |
|---|---|---|---|
| $(V/R)/(V/R)_{ref}$ | 1.40 | 1.41 | 1.59 |

**Table 1: Vertical velocities at the rotor disk for different $C_T$ cases**

ii. For a different case $C_{T_{req}} = C_{T_2} \neq C_{T_{ref}}$, that same distance would be traveled at different time and thus reached at a different $\psi_2$ which can be calculated as follows:

$$\Delta \tilde{z} = \Delta \tilde{z}_{ref} = \text{constant} \quad \Rightarrow \frac{V_2}{\psi_2} = \frac{V_{ref}}{\psi_{ref}} = \text{constant}$$

$$\Rightarrow \frac{\psi_2}{\psi_{ref}} = \frac{V_2}{V_{ref}} = \sqrt{\frac{C_{T_2}}{C_{T_{ref}}}}$$

(11)

iii. We may now generalize for any $\psi_{ref}$, using the reference point: $C_{T_{ref}} = 0.008$, to get the factored time step $\psi_*$:

$$\psi_* = \sqrt{\frac{C_{T_*}}{C_{T_{ref}}}} \cdot \psi = \sqrt{\frac{C_{T_{req}}}{0.008}} \cdot \psi$$
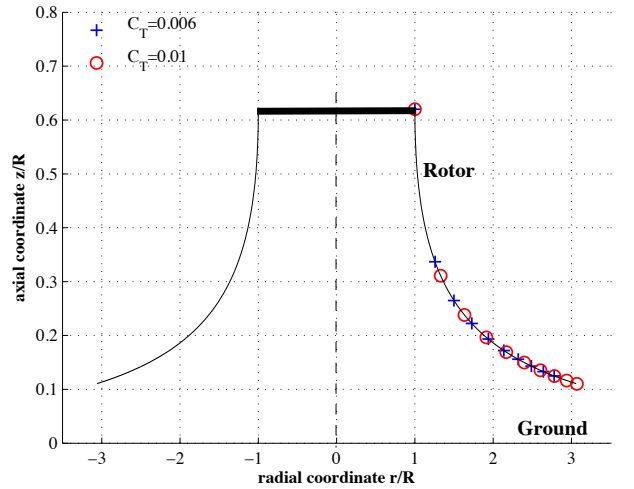
(12)



**Fig. 10: Effect of $C_T$ on prescribed trajectory at $Z/R = 0.62$**

Figure 10 portrays a representation of this practice, showing faster advancement of tip vortices along the prescribed trajectory (represented by the points) for a higher $C_T$ case *i.e.* higher downwards velocity at the rotor plane and as such the gaps between the points grow larger.

Finally, the equations describing tip vortex geometry in ground effect for $Z/R \leq 0.6$ can be written as:

$$\tilde{r}_{tip}(\psi_*) = \frac{r_{tip}(\psi_*)}{R} = (-0.00025\psi_*^2 + 0.0485\psi_* + 1) \quad (13)$$

and

$$\tilde{z}_{tip}(\psi_*) = \tilde{z}_{tip}\left(\tilde{r}_{tip}(\psi_*)\right) \quad = \frac{z_{tip}\left(\tilde{r}_{tip}(\psi_*)\right)}{R}$$

$$= Z/R[-1 + e^{(-1.2035\sqrt{\tilde{r}_{tip}(\psi_*)-1})}] \quad (14)$$

To complete the formulation for the proposed prescribed wake method in ground effect, a mirror image rotor wake was implemented, causing a no-penetration condition at the ground plane. The illustration in Figure 11 presents a single tip vortex trajectory for both the primary and mirror rotors, as well as a 30° near-wake for 5 representative blade elements (reduced for image clarity), where each pair of points defines one straight vortex filament.
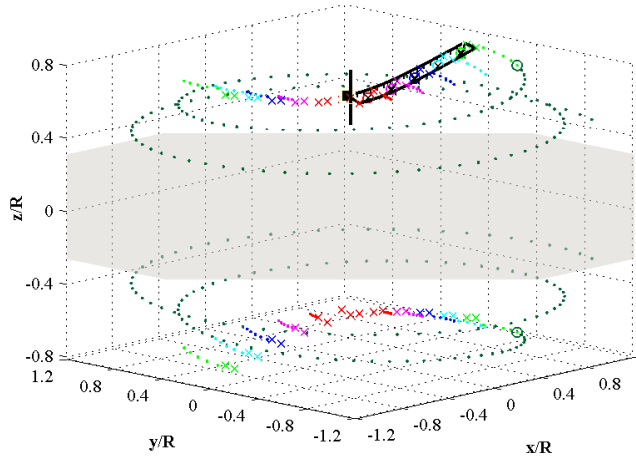


**Fig. 11: Illustrated prescribed wake of an elastic rotor at $Z/R = 0.62$ and its mirror image. Ground plane shown as shaded area**

The sensitivity studies performed on the OGE formulation (as described above) were repeated for the IGE methodology with similar results. Sensitivity to trajectory shapes was also examined, showing that the power results to be somewhat sensitive to constant variation in vertical displacements of the wake shape, yet a rather negligible sensitivity to variations in the wake's curvature shape. Figure 12 shows several wake shape variations that were examined alongside the respective power differences with respect to the reference case demonstrating said conclusions (note that the axes are scaled differently).

## Prescribed Wake Validation in and out of Ground Effect

To justify the proposed approach and validate its predictive capability, calculated results were compared to experimental results from a range of experiments, including both in-house test rotors.

**Prescribed Wake Validation OGE**

Initial validation was carried out based on AH-1G main rotor flight test measurements presented by Kocurek and Tangler
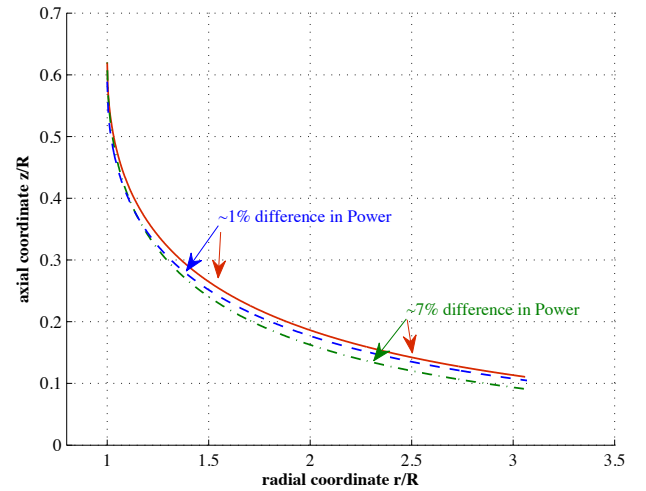


**Fig. 12: Variation in trajectory shapes and their effect on power at $Z/R = 0.62$**

[24], using the prescribed wake model given in the same body of work as described above. The rotor performance comparison shown in Figure 13 displays very good correlation between the current formulation results and the experimental data.

Further validation was successfully carried out using data from our sub-scale test at $Z/R = 2$, considered as OGE condition, and is presented in Figure 14. Again, the correlation of calculated and measured results is quite good.
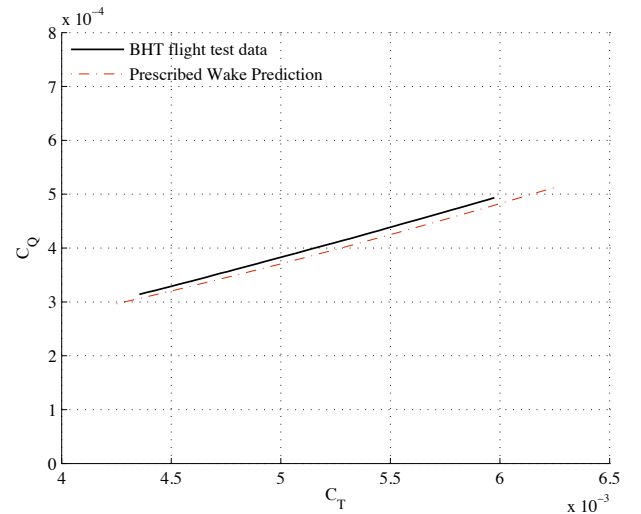


**Fig. 13: Prescribed wake vs experimental results for hover performance for an AH-1G Main rotor OGE**

**Prescribed Wake Validation IGE**
The proposed prescribed wake analysis in ground effect was validated using data from our sub-scale test set up (rigid rotor). Computational results were compared to experimental results at four RPM cases at $Z/R = 0.1$. As seen in Figure 15, the power prediction over the range of tested thrust cases showed good correlation with the experimental results. Further validation is given in Figure 16, successfully comparing total power ratios, $P_{IGE}/P_{OGE}$, extracted using the prescribed wake IGE method
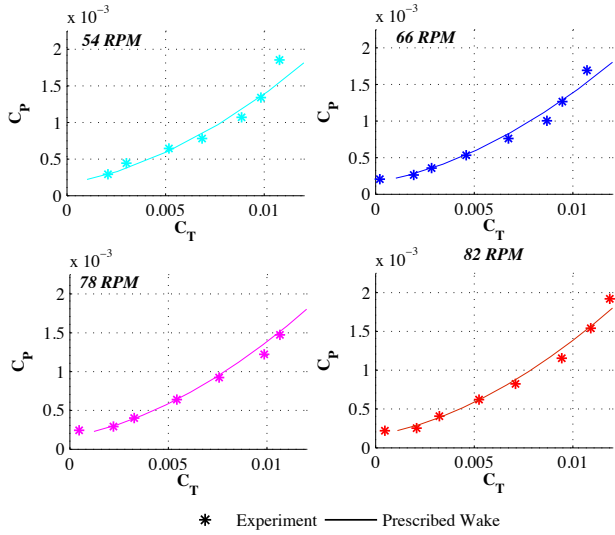
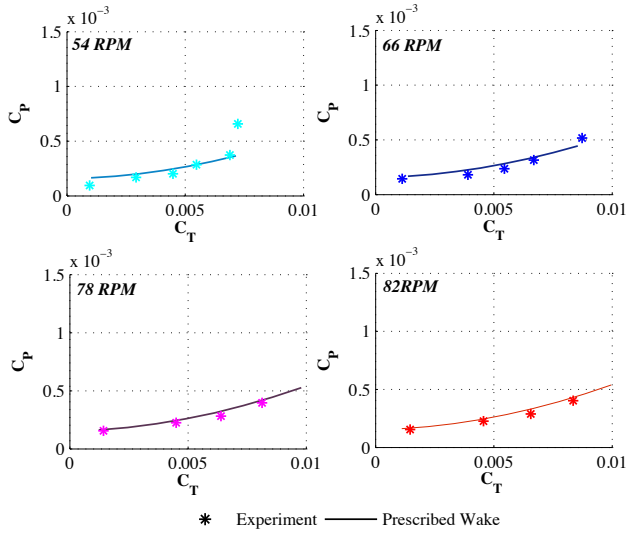**Fig. 14: Prescribed wake vs experimental results for sub-scale test OGE**



**Fig. 15: Prescribed wake vs experimental results IGE for the sub-scale test at** $(Z/R)_{hub} = 0.1$
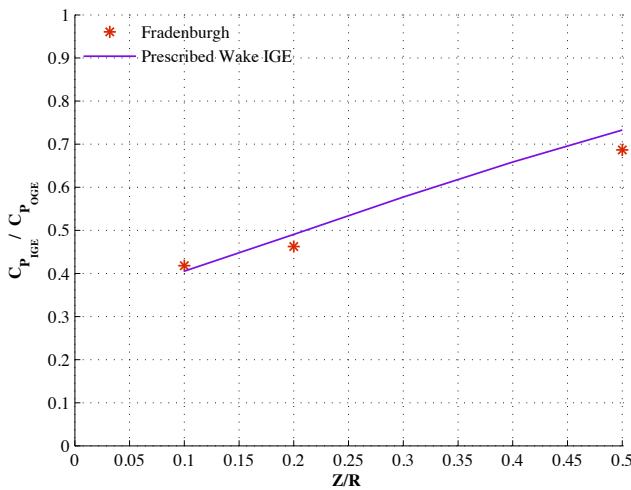


**Fig. 16: Total power ratio IGE for constant thrust - prescribed wake vs experimental results**

to experimental results by Fradenburgh [7] for $Z/R$ of less than 0.5 and $C_T/\sigma = 0.06$.
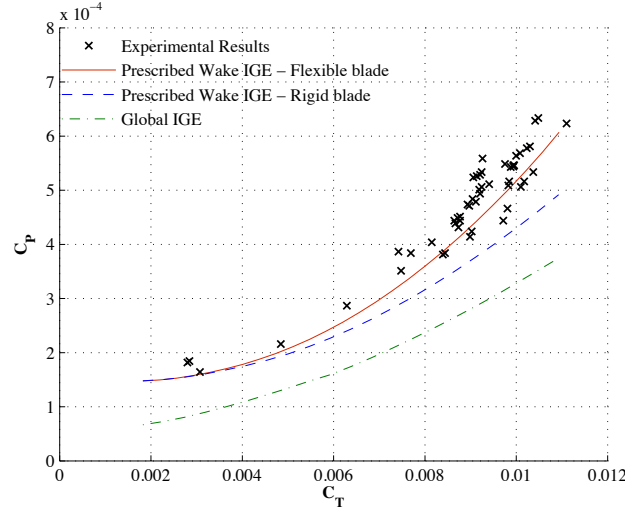


**Fig. 17: Prescribed wake vs experimental results IGE for the full scale rotor at** $(Z/R)_{hub} = 0.1$

Further, results using this method were compared to experimental data from our full scale, highly flexible, rotor test set-up for two different heights off ground. Figure 17 presents experimental results for $(Z/R)_{hub} = 0.1$ at 18 *RPM* against computational results for both rigid and flexible blade modeling assumptions. The comparison clearly conveys an improved correlation to test results when accounting for blade flexibility, especially at high thrust levels. The figure also shows a curve for global IGE modeling, where the OGE power results are factored for ground effect using the global $P_{IGE}/P_{OGE}$ ratio correlating with $(Z/R)_{hub} = 0.1$. The latter considerably under-predicts the experimental power data. It can be easily concluded from this comparison that predictive quality is significantly increased by considering the effect of $Z(\tilde{r})/R$ distribution caused by substantial blade deflections in ground effect.
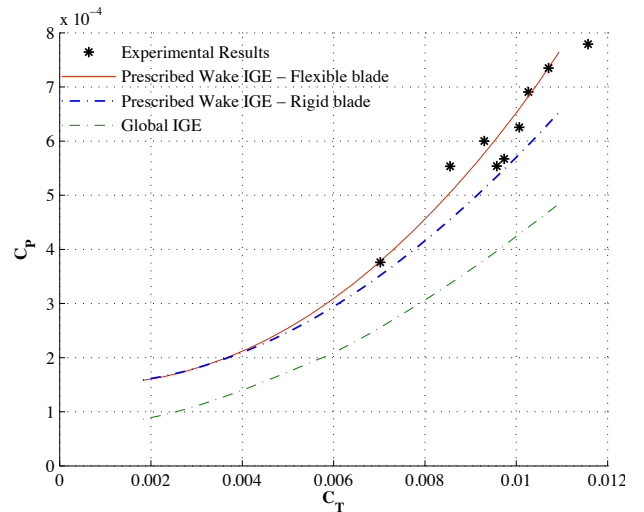


**Fig. 18: Prescribed wake vs experimental results IGE for the full scale rotor at** $(Z/R)_{hub} = 0.2$

A similar comparison between experimental results and the computational results is shown in Figure 18 for the same ex-

perimental set up at the height of 130 *cm* $((Z/R)_{hub} = 0.2)$. Here too, a very good agreement is shown between the test data and the prescribed wake model, once again showing improved agreement using the flexible blade model. Also similarly to the previous case, a poor under-predicting correlation is observed when using global implementation of empirical power ratio factors.

## Results for Full Scale Flexible Rotor in Extreme Ground Effect

After the validation studies described above, the new approach was employed towards a parametric study examining the performance of a highly flexible rotor in extreme ground effect. The effects of blade stiffness, RPM, planform taper, and linear blade twist were examined using the full scale rotor geometry and airfoil at the operational height of $Z/R_{hub} = 0.1$.

**Effect of Blade Stiffness**
Rotor performance in this unusual environment was studied at various blade stiffnesses to isolate the effect of increasing flexibility. The actual blade stiffness obtained via static cantilevered bending tests was used as a baseline (100% stiffness). Figure 19 shows power vs thrust for the rotor using rigid blades, baseline elastic blades, and blades of 200% and 50% of baseline stiffness. The results clearly demonstrate that in these extreme ground effect conditions, a softer blade in bending will inflict higher power losses, due to loss of ground effect and thus loss of related performance benefits. The difference in performance characteristics becomes more substantial with increasing thrust which in turn increases bending deflections.
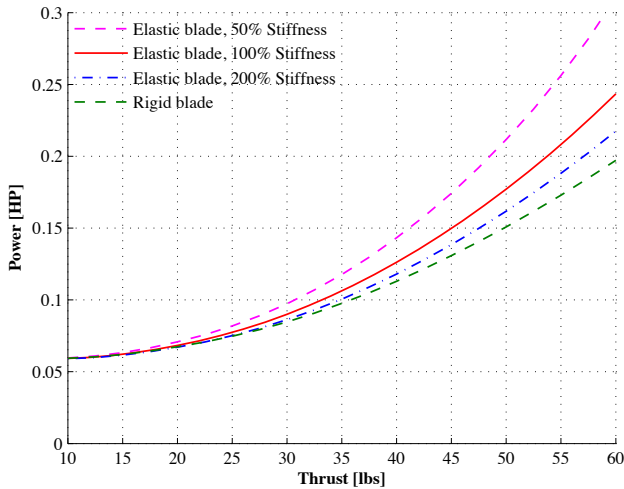


**Fig. 19: Effect of elasticity on full scale rotor performance IGE at** $(Z/R)_{hub} = 0.1$ **and** 18 *RPM*

**Effect of RPM**
Rotor RPM was examined at three thrust levels of 30 *lbs*, 40 *lbs*, and 50 *lbs* per rotor, respectively representing $C_T$ of 0.0055, 0.0073, and 0.0091. Lower RPM values are usually accompanied by higher angles of attack, which results in stall over inboard blade elements, and thus increase in power. On the

other hand, rotating at higher RPM values inherently increases profile drag. Thus, a minimum power RPM value exists, and can be seen in Figure 20 for the three different load cases at the operational height of $(Z/R)_{hub} = 0.1$. The RPM value for minimum power increases with thrust because of higher angle of attack requirements at higher loading, which facilitates the onset of blade stall.

Apparent from this study as well is the effect of blade flexibility (all three load cases use the same blade stiffness value). The difference between power requirements for flexible and rigid blades noticeably increases with thrust, which is expected due to increased blade deflections causing loss of ground effect benefits (as demonstrated in Figure 19). Also, a slight decrease in power loss due to flexibility can be seen with increase in RPM due to the effect of centrifugal forces stiffening the blades.
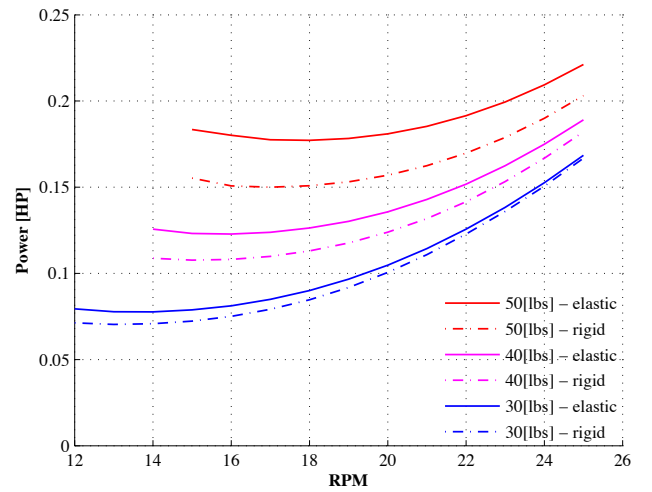


**Fig. 20: Effect of RPM on full scale rotor performance IGE at** $(Z/R)_{hub} = 0.1$ **and** 18 *RPM*

**Effect of linear planform taper** The effect of linear planform taper was studied as the chord distribution was varied while maintaining a constant thrust weighted solidity [2]. The taper ratio (root chord over tip chord) was increased from a rectangular planform up to a taper ratio of 5 : 1. Shown in Figure 21 are power vs taper ratio results at the same three thrust levels mentioned above, for both rigid and flexible rotors. The results show power reductions up to 15% as taper ratio increases, for both the rigid and elastic blades.

These results are explained via the extraction of lift coefficient as described in (5). The wake geometry is barely influenced by the planform taper, the only effect being the slight geometric variations in the three-quarter chord positions and trailing vortices points of origin. Therefore, the circulation distribution along the blade remains mostly similar. For a similar circulation distribution, the lift coefficient is inversely dependent on blade chord, and is calculated as follows:

$$\bar{C}_l(\tilde{r}) = \frac{2\overline{\Gamma}(\tilde{r})}{U \cdot \bar{c}(\tilde{r})} \qquad (15)$$

As a result, the lift distribution along the blade approaches a more uniform distribution, offloading the outboard blade el-
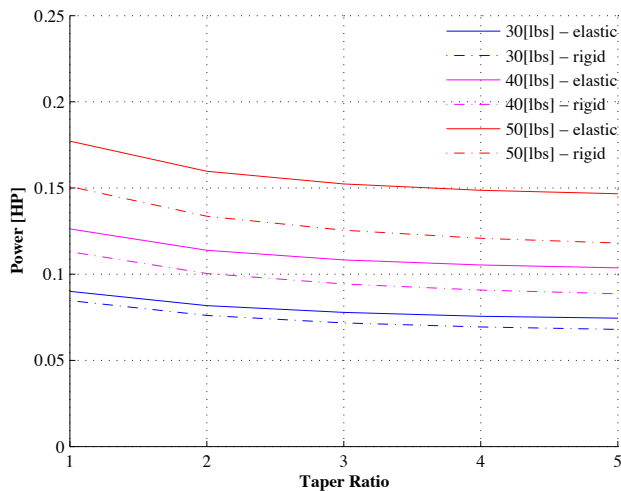
**Fig. 21: Effect of planform taper on full scale rotor performance IGE at** $(Z/R)_{hub} = 0.1$ **and** $18 \, RPM$



**Fig. 22: Effect of linear twist on full scale rotor performance IGE at** $(Z/R)_{hub} = 0.1$ **and** $18 \, RPM$

ements, therefore resulting in decreased power requirements. Within airfoil stall limits, as a stronger taper ratio is applied, the loading on the blade becomes more uniform which decreases torque, and thus power.

The effect of taper appears to be increased in extreme ground effect, relative to the expected few percentages $(2\% - 4\%)$ of power savings for conventional rotors hovering out of ground effect [15], and is attributed mainly to profile power. Since as discussed above, induced power decreases significantly with inflow in extreme ground effect, the relative part of profile power in total power becomes larger. Thus savings in profile power as a result of blade taper are substantially more pronounced in this case.

The influence of blade flexibility can be observed here too, as the difference in power requirements between the rigid and flexible rotors decreases with the thrust level and resulting deflection.

**Effect of linear twist** Lastly, the influence of linear blade twist on rotor performance was investigated, and is shown in Figure 22 for the same three levels of thrust as above. The results indicate a minor effect of blade twist on power requirements, diminishing with the increase of thrust (where on average the angles of attack increase nearing closer to stall). It is also apparent that twist is less effective on the flexible blade compared to the rigid blade, and the optimum twist for minimum power is smaller. This is because the blade elasticity already accounts for some torsion without pre-twist.

It should be noted that for this prescribed wake model blade twist is implemented only on a geometric level, unlike OGE prescribed wake models, such as [22] and [24], which also include the effect of blade pre-twist in the functions describing the wake trajectory. In this model, blade twist only affects the geometric three-quarter chord positions and trailing vortices points of origin. Therefore it is understood that the results for the influence of linear twist on performance are incomplete.
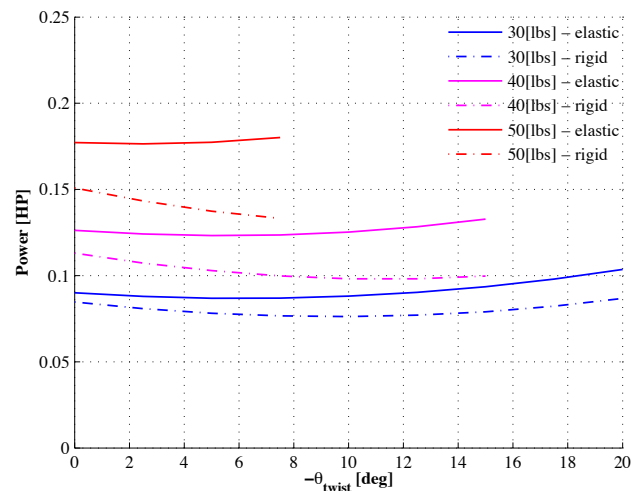
## Conclusions

This study was conducted towards designing an ultra-lightweight, and therefore highly elastic, rotor blade for the quad-rotor attempt at the Sikorsky human powered helicopter challenge. A new approach for performance prediction of a highly flexible rotor in extreme ground effect was developed, using a new prescribed wake model representing tip vortex trajectories in ground effect and a mirror image rotor representing the ground condition. Two new sets of experimental results for rotor performance in extreme ground effect were presented. The first set-up includes a rigid sub-scale rotor $(R = 1.26 \, m)$ operating in the regime of $0.06 \leq Z/R \leq 2.0$. The second experiment uses the full-scale HPH rotor $(R = 6.5 \, m)$, tested at $Z/R = 0.1$ and $Z/R = 0.2$. The computational process was extensively validated for both the rigid and highly elastic rotors, in and out of ground effect, using the new experimental data along side experimental measurements from the literature.

A parametric study was carried out showing the effects of various rotor design variables on performance in extreme ground effect for both a rigid and a highly elastic blade. It was shown that blade stiffness has a high impact on performance in ground effect, as the highly flexible rotor requires substantially more power in hover at $(Z/R)_{hub} = 0.1$. For example 15% more power is needed at the thrust level of $50 \, lbs$ for the baseline stiffness case than that of a rigid rotor. It was also shown that the power loss increases as stiffness decreases.

The effect of rotor RPM was examined leading to the conclusion that the RPM for minimum power increases with the thrust level. This study showed that careful selection of operational RPM can save up to 20% in power requirements using both rigid and flexible rotors (comparing $24 \, RPM$ to $18 \, RPM$ for $50 \, lbs$ of thrust). Studying the effect of planform taper for this rotor resulted in significant power savings as well, 15% savings in power requirements were demonstrated for the $50 \, lbs$ thrust level when implementing a 3:1 planform taper ratio. Lastly, the relative effect of blade twist on the rigid and flexible blades was studied, showing that pre-twist is less effective on the deflected blade.

Throughout the parametric studies, the effect of stiffness was apparent showing that required power increases for a flexible rotor in hover, relatively to a rigid rotor. This effect increases with thrust requirements, due to the higher deflections and associated loss of ground effect. Thus, it is proved that careful consideration of blade deflections when modeling flexible rotor performance in extreme ground effect is key to successful prediction capabilities.

This new predictive method will be used for an optimized redesign of the HPH rotor, towards further pursue of the Sikorsky Human Powered Helicopter Challenge.

## Acknowledgments

## References

[1] Abe K. Kawasima T. Motohashi T. Goto H., Kato D. and Naito A. Power measurements of yuri i. Technical report, 1994.

[2] Leishman J. G. *Principles of Helicopter Aerodynamics*. Cambridge University Press, 2006.

[3] Filippone A. On the possibility of human-powered vertical flight. *Journal of the American Helicopter Society*, 52(4):371–382, 2007.

[4] Hawkins T. J. Aerodynamic and power considerations for human powered helicopter in vertical flight. Master's thesis, Stanford University, March 1996.

[5] Knight M. and Hefner R.A. Analysis of ground effect on the lifting airscrew. Technical report, 1941. NACA TN-835.

[6] Zbrozek J. Ground effect on the lifting rotor. Technical report, 1947. British R & M No. 2347.

[7] Fradenburgh E. A. The helicopter as a ground effect machine. volume 1, 1959. Symposium on Ground Effect Phenomena, Princeton University, Princeton, NJ.

[8] Fradenburgh E. A. The helicopter and the ground effect machine. *Journal of the American Helicopter Society*, 5(4):26–28, 1960.

[9] Koo J. and Oka T. Experimental study on the ground effect of a model helicopter rotor in hovering. Technical report, 1971. NASA TT F-13938, Translation of Report NAL-TR-113.

[10] Bellinger D. E. Experimental investigation of effects of blade section camber and planform taper on rotor hover performance. Technical report, 1972. UARL TR724.

[11] Hayden J.S. The effect of the ground on helicopter hovering power required. 1976. American Helicopter Society 32$^{nd}$ Annual Forum Proceedings.

[12] Leishman J.G. Lee T.E. and Ramasamy M. Fluid dynamics of interacting blade tip vortices with a ground plane. 2008. American Helicopter Society 64$^{th}$ Annual Forum Proceedings.

[13] Lighthill J. A simple fluid-flow model of ground effect on hovering. *Journal of Fluid Mechanics*, 93(4):781–797, 1979.

[14] Cheeseman I. C. and Bennet W. E. The effect of the ground on a helicopter rotor in forward flight. 1955. ARC R&M 3021.

[15] Johnson W. *Helicopter Theory*. Dover Publications, Inc., 1994.

[16] Griffiths D. A. and Leishman J. G. A study of dual-rotor interference and ground effect using a free-vortex wake model. 2002. American Helicopter Society 58$^{th}$ Annual Forum Proceedings.

[17] Ananthan S. *Analysis Of Rotor Wake Aerodynamics During Maneuvering Flight Using a Free-Vortex Wake Methodology*. PhD thesis, University of Maryland, 2006.

[18] Lakshminarayan V. K. Kalra T. S. and Baeder J. D. CFD validation of micro hovering rotor in ground effect. 2010. American Helicopter Society 66$^{th}$ Annual Forum Proceedings.

[19] Khromov V. and Rand O. Ground effect modeling for rotary-wing simulation. 2008. 26$^{th}$ International Congress of the Aeronautical Sciences.

[20] O. Rand. A phenomenological modification for glauert's classical induced velocity equation. *Journal of the AHS*, 51(3):279–282, 2006.

[21] Selig M.S. and McGranahan B.D. Wind tunnel aerodynamic tests of six airfoils for use on small wind turbines. Technical report, 2004. NREL/SR-500-34515.

[22] Landgrebe A. J. An analytical and experimental investigation of helicopter rotor hover performance and wake geometry characteristics. Technical report, 1971. USAAMRDL TR 71-24.

[23] Landgrebe A. J. The wake geometry of a hovering helicopter rotor and its influence on rotor performance. *Journal of the American Helicopter Society*, 17(4):3–15, 1972.

[24] Kocurek J. D. and Tangler J. L. A prescribed wake lifting surface hover performance analysis. 1976. American helicopter Society 32$^{nd}$ Annual Forum Proceedings.

[25] Light J. S. Tip vortex geometry of a hovering helicopter rotor in ground effect. 1989. American helicopter Society 45$^{th}$ Annual National Forum of the .